Journal of Alloys and Compounds 516 (2012) 167–171

Contents lists available at SciVerse ScienceDirect

Journal of Alloys and Compounds

journal homepage: www.elsevier.com/locate/jallcom

Comparative study of critical current density, pinning force and levitation force behavior in Yb211 doped-Sm123 bulk superconductors

K. Ozturk[a,*], S. Akbulut[a], S. Kutuk[a], S. Bolat[a], S. Celik[b], M. Basoglu[a]

[a] Department of Physics, Faculty of Arts and Sciences, Karadeniz Technical University, 61080 Trabzon, Turkey
[b] Department of Physics, Faculty of Arts and Sciences, University of Rize, 53100 Rize, Turkey

ARTICLE INFO

Article history:
Received 20 June 2011
Received in revised form
30 November 2011
Accepted 8 December 2011
Available online 17 December 2011

Keywords:
High-T_c superconductor
Critical current
Compositional fluctuation
Flux pinning

ABSTRACT

The effect of Yb211 doping on the critical transition temperature (T_c), *c*-lattice parameter, critical current density (J_c), volume pinning force (F_p) and the vertical levitation force density properties of MPMG-processed $(Sm123)_{1-x}(Yb211)_x$ samples were investigated. In this study the $(Sm123)_{1-x}(Yb211)_x$ sample with $x = 0.25$ shows the best $J_c(0)$ value which is almost five times larger than that of the undoped one at zero field and at 77 K, though in the peak effect region the best J_c performance has the sample with $x = 0.05$ Yb211 doping ratio. $J_c(H)$ curves exhibits a wide plateau ranging from 0.75 to 2.75 T at 77 K with Yb211 doping ratio for $0.05 \leq x \leq 0.20$ pointing out that the $(Sm123)_{1-x}(Yb211)_x$ samples presented here are attractive for superconducting application especially under high magnetic fields.

© 2011 Elsevier B.V. All rights reserved.

1. Introduction

The most promising fields for potential application of the high-temperature superconductors (HTS) are large scale power applications such as superconducting magnets, superconducting bearings as an energy storage systems, power cables, and MAGLEV transportation systems [1–3]. Almost all these applications require a high current density under magnetic field flowing at acceptable low dissipation in liquid nitrogen temperature. Unfortunately, J_c is disappointing low of high-temperature superconductors based on the RE—Ba—Cu—O compounds (where RE is a rare-earth-elements, such as Dy, Gd, Nd, Sm, and Y), because of ceramic character of these materials with its granular structure and the appearance of the weak-links problem, generally occurring at grain boundaries [4–6]. Since the discovery of high temperature superconductivity, a variety of attempts have been carried out to enhance the critical current density J_c and to optimize the critical temperature T_c of the superconductor for technological applications. It is well known that achieving high J_c, irreversibility field B_{irr} and magnetic field trapping ability in high temperature superconductors requires effective flux pinning. Therefore, several preparation techniques were developed to enhance pinning properties of HTS such as melt-textured growth (MTG) [7], liquid phase process [8], powder melting process (PMP) [9], melt powder melt growth (MPMG) [10], and top-seeded melt-growth (TSMG) [11,12] process.

In many research center, various kinds of chemical doping, including metal and nonmetal elements particles of magnetic alloys [13–16], various insulating particles such as RE_2BaCuO_5 (RE211) and $RE_2Ba_4CuO_5$ (RE-2411) and other nonsuperconducting particle have been used as secondary phase particles which can be act as pinning centers in bulk HTS superconductors [17–19]. It is well known that, compared to $YBa_2Cu_3O_{y-\delta}$ the (LRE)$Ba_2Cu_3O_{7-\delta}$ superconductors, where LRE is a light rare earth element, such as La, Nd, Sm, Eu and Gd, attract important attention as a consequence of their higher superconducting transition temperature (T_c) and critical current density (J_c), especially in medium and strong magnetic fields. However, due to a close size difference between LRE^{3+} and Ba^{2+} ions, the light rare earth elements can easily substitute Ba, resulting in the formation of $LRE_{1+x}Ba_{2-x}Cu_3O_{7-\delta}$ solid solution. As a result, this substitution causes a reduction in T_c and a broadening of the superconducting transition interval [20]. It was reported that to overcome this drawback, the oxygen controlled melt growth (OCMG) process was developed successfully, consisting of synthesizing the LRE123 material under low partial oxygen pressure (1% or 0.1% O_2 in Ar ambient) [21]. Alternatively, to suppress the LRE/Ba substitution and to enhance T_c and the superconducting properties of the (LRE)123 bulk with the melt-texture-growth (MTG), various Ba-rich additions, such as $Sm_2Ba_4Cu_2O_9$ (Sm242) and Sm_2BaO_4 (Sm210) have been used [19,22]. It was also pointed out that mixed rare-earth compounds are more favorable than single rare-earth compounds because a better controlled growth of

* Corresponding author. Tel.: +90 462 377 41 54; fax: +90 462 377 31 95.
E-mail address: kozturk@ktu.edu.tr (K. Ozturk).

0925-8388/$ – see front matter © 2011 Elsevier B.V. All rights reserved.
doi:10.1016/j.jallcom.2011.12.021

superconductor material and enhanced pinning properties through formation of local strain fields arising from the differences in ionic sizes of the rare-earth elements, such as Yb, Tm and Er [16,23,24]. It was also reported that the feature of compositional fluctuation regions, which induce pinning centers needed for higher critical current in superconductor, could be altered by differences in peritectic temperature, solubility in liquid phase, and ionic radius [25].

It is also well known that the microstructure characteristics of bulk RE123 superconductor composites control their physical properties. Therefore, the understanding and control of the microstructure are attractive challenges to enhance the superconducting properties of MPMG-processed Sm123 sample. Our previous studies indicated that the doping of Yb211 (Yb_2BaCuO_5) into the Sm123 superconductor sample increases the value of the vertical magnetic levitation force [26]. The main objective of this study is to determine the relations between critical current density, volume magnetic pinning force, magnetic levitation force (in zero field cooling regime) and pinning mechanism of the bulk superconductor samples with nominal composition of $(Sm123)_{1-x}(Yb211)_x$ depending on non-superconducting Yb211 doping ratio x, varying from 0.00 to 0.35. The second aim is to investigate the influence of the fabrication temperature of $(Sm123)_{1-x}(Yb211)_x$ samples on levitation force and pinning properties. Therefore, in this study the measurements of field-dependent magnetization, resistivity ρ, volume magnetic pinning force, magnetic levitation force, pinning mechanism and microstructural analysis were performed to further understand the effect of Yb211 doping on the superconducting properties of the nominal $(Sm123)_{1-x}(Yb211)_x$ samples.

2. Experimental

Firstly, high purity commercial Sm_2O_3, $BaCO_3$, CuO and Yb_2O_3 powder are weighed to have a nominal composition of $SmBa_2Cu_3O_{7-\delta}$ and Yb_2BaCuO_5, which are denoted as Sm123 and Yb211 thereafter, respectively. The polycrystalline Sm123 sample is prepared by the MPMG method, while Yb211 powder to dope into Sm123 superconductor is prepared by the solid-state reaction technique (SSR). After the stoichiometric mixture of Sm_2O_3, $BaCO_3$ and CuO is thoroughly ground for half an hour the powder in the Pt-crucible is placed into a furnace for 5 min at a temperature of 1460 °C. Then, the sample is immediately cooled down to the room temperature. After the quenched samples are ground and mixed well the Yb211 powder is added to the Sm123 powder to have nominal composition of $(Sm123)_{1-x}(Yb211)_x$ structure for x = 0.00, 0.05, 0.10, 0.15, 0.20, 0.25 and 0.35 and this powder is mixed well again. Following this procedure, Yb211-doped and undoped powders are pressed into a pellet form with 13 mm in diameter under 400 MPa pressure. Then, to understand whether the reheating temperature and cooling speeds have an effect on superconducting levitation force or not $(Sm123)_{1-x}(Yb211)_x$ samples are heated to 1170 °C (reheating temperature) which is different than our earlier produced Sm123 samples [26]. After that, the samples were held at this temperature for 15 min and cooled down to 980 °C at the speed of 1.7 °C/min. This process was followed by slow cooling with a rate of 0.02 °C/min down to 880 °C and finally the samples were cooled to room temperature at the rate of 2 °C/min. At the final stage of the cooling, the samples are subjected to oxygenation at 500 °C for four hours, then cooled down to 300 °C at the rate of 2 °C/min under oxygen flow, and finally, the cooling process was continued to room temperature at the rate of 5 °C/min.

Magnetization hysteresis loops (M–H) were measured using a vibrating sample magnetometer (VSM) of the Quantum Design PPMS system at temperatures such as 5, 50 and 77 K with the magnetic field applied perpendicular to the sample surface. The measurements were performed by the sweep rate of 5 mT s^{-1}. All resistance measurements in PPMS system after ZFC regime were carried out at constant magnetic field, varying the temperature from 50 to 100 K in steps of 0.25 K with a heating rate of 3 K min^{-1}. All samples were rectangular and typical dimensions were 1.1 mm × 2.1 mm × 9.0 mm and 0.5 mm × 3.2 mm × 2.6 mm for electrical resistivity and magnetization studies respectively.

The microstructure of the samples was investigated by an optical microscope and a scanning electron microscope (SEM, Zeiss Evo LS10) equipped with an EDX analyzer. The X-ray diffraction (XRD) data were collected using a Rigaku D/Max-IIIC diffractometer with Cu Kα radiation over the range 20–60° with a step 0.02° and a scan speed 2° min^{-1} at room temperature. The orthorhombic lattice parameters (a–c) were calculated from (0 0 6), (0 2 0), (2 0 0), (0 1 3), (1 0 3) and (1 1 6) peaks using least square methods.

The levitation force measurements of the samples at liquid nitrogen temperature were performed using a self-made device. Details were reported elsewhere [27]. Vertical forces between the bulk HTSs and cylindrical NdFeB Permanent magnet (PM) were measured for zero field cooling (ZFC) regime at 77 K. The cylindrical PM, which is used in the measurement of vertical force vs. vertical distance, has a diameter of 13 mm, a thickness of 6 mm and a magnetic field of 0.5 T in the center of the top surface of the PM. The levitation force experiment is performed by first placing the bulk sample at the same cooling height and approximately over the center of top surface of the PM. The magnet is moved toward to or away from the superconductor sample by a servo motor. The vertical distance and vertical force are measured by using a displacement sensor and load cells, respectively. The vertical forces vs. vertical distance of the bulk samples are measured continuously, controlled by PC and the movement rate of the PM for force measurement is fixed to be 2 mm/s.

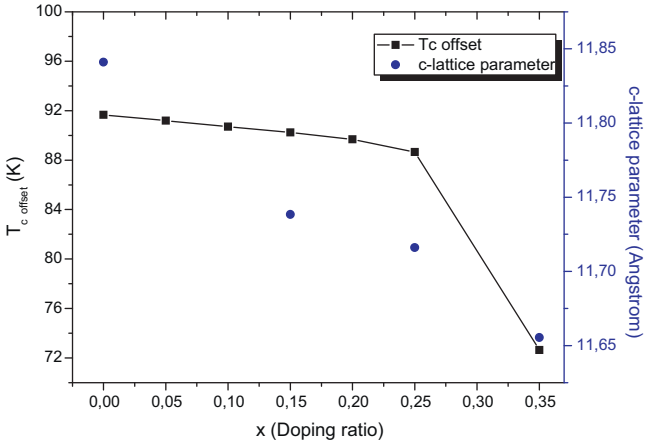

Fig. 1. The variation of the transition temperature $T_{c\ offset}$ and c-lattice constant of nominal $(Sm123)_{1-x}(Yb211)_x$ bulk samples depending on Yb211 doping ratio x.

3. Results and discussion

In order to obtain a better understanding of the effects of Yb211 doping on the formation of Sm123 superconductor compound with increasing doping level x, XRD measurements were performed on the nominal $(Sm123)_{1-x}(Yb211)_x$ samples. The Yb211 doping ratio dependence of the $T_{c\ offset}$ and the c-lattice constant of nominal $(Sm123)_{1-x}(Yb211)_x$ bulk samples (reheating temperature 1170 °C) with x = 0.00, 0.05, 0.10, 0.15, 0.20, 0.25 and 0.35 are shown in Fig. 1. It is found that although the crystal structure of the samples kept their orthorhombic form, the value of c-lattice constant reduces with increasing x similar as reported in a former study, in which the reheating temperature was 1100 °C [27]. In our study, the decrease of the c-lattice constants with increasing Yb211 doping ratio shows that Yb^{3+} ions with small ionic size partly substitute for Sm^{3+} ions with relatively large ionic size [16,28]. In addition, a combination of (Sm,Yb)123, Yb123 and Sm123 superconducting phases form in the main superconductor matrix (in literature values of c-lattice constants of 11.65 and 11.76 Å were reported for Yb123 and Sm123 bulk superconductors respectively [28,29]). It is also known that the peritectic temperature of Yb123 is lower than that of Sm123 and therefore, Yb123 and (Sm,Yb)123 are formed during the Sm123 growth. It was found that superconducting transition width broadens with increasing of Yb211 doping ratio. This broadening indicates that the Yb211 doping induces a fluctuation of the T_c in the Sm123 sample. It is also seen from Fig. 1 that the value of $T_{c\ offset}$ decreases gradually up to the value of x = 0.25 and after that decreases rapidly with increasing of x doping ratio. The rapid decrease of $T_{c\ offset}$ for x = 0.35 can be explained by the excess of the non-superconducting phases amount in superconductor sample [22,29].

To illuminate the origin of the pinning force, the critical current and the levitation force improvement, we observed the microstructure and performed a quantitative analysis by SEM-EDX. It was seen in both former and current SEM images that the average grain size of $(Sm123)_{1-x}(Yb211)_x$ samples were about 15–45 μm and that the

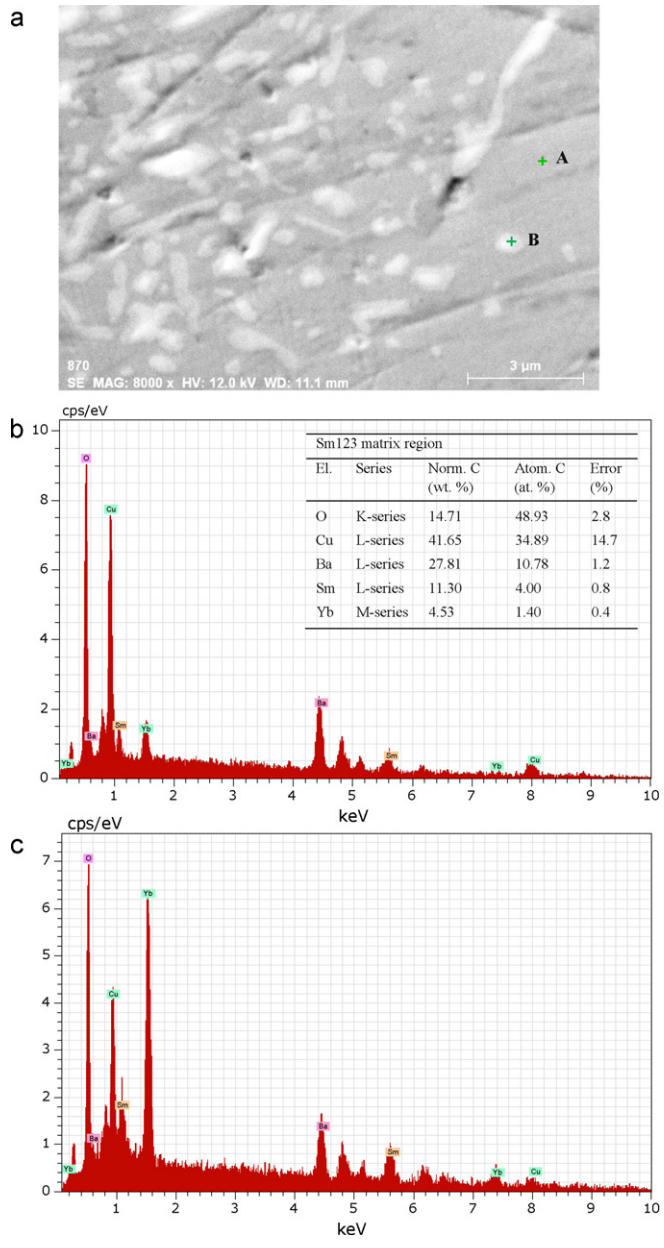

Fig. 2. (a) The SEM image of $(Sm123)_{1-x}(Yb211)_x$ samples taken from 10 μm depth of upper surface and (b) the electron dispersive X-ray (EDX) spectra taken from Sm123 matrix on point A and (c) secondary phase regions on point B of Yb211-doped bulk Sm123 sample for doping ratio $x = 0.25$. In (b) also the compositional analysis data taken from Sm123 matrix region is shown.

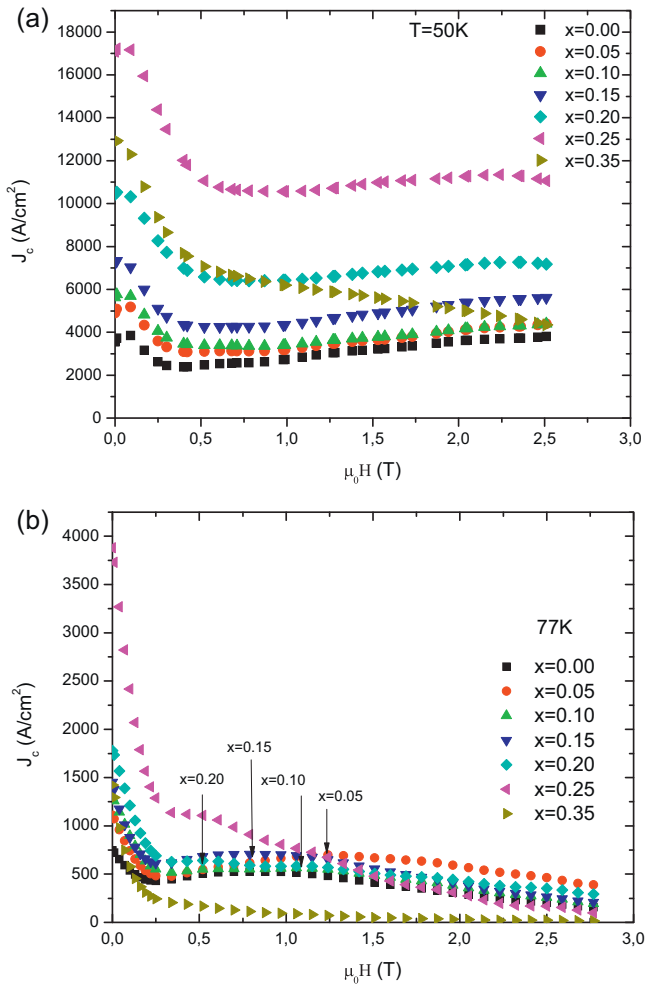

Fig. 3. Magnetic field dependence of the critical current densities of $(Sm123)_{1-x}(Yb211)_x$ sample for doping ratio of $x = 0.00$, 0.05, 0.10, 0.15, 0.20, 0.25 and 0.35 at (a) 50 K and (b) 77 K measurement temperatures.

superconductor matrix contains pores and cracks of different size. The SEM image of $(Sm123)_{1-x}(Yb211)_x$ samples and the electron dispersive X-ray (EDX) spectra taken from Sm123 matrix (point A) and secondary phase region (point B in Fig. 2(a)) are shown in Fig. 2. The compositional analysis data taken from Sm123 matrix region shown in Fig. 2(b) point out that the matrix region is composed of Sm123 and (Sm,Yb)123 superconducting phases. As shown in Fig. 2(a) and (c), the light regions indicate the RE211 particles (as Yb211 and Sm211) trapped inside the Sm123 matrix with dark regions. The size of the Yb211 and Sm211 particles for $x = 0.25$ doping ratio are estimated to be between 0.5 and 2 μm. It was also observed that, with increasing of the Yb211 doping, the number density of RE211 particles in the Sm123 matrix increased. The detailed EDX compositional analysis results showed that the atomic percentage of Yb increases while the percentage of Sm decreases with the increasing of Yb211 doping ratio both in the intergrain and secondary phase regions (point B in Fig 2(a) and (c)) compared with those in the Sm123 matrix region. From the EDX analyses we found secondary phases in the sample such as $BaCuO_2$, Yb211, Sm211 and RE_2O_3.

The $J_c(H)$ values of the samples were obtained from the M–H loops using the extended Bean model with the following relation: $J_c = 20\Delta M/[a(1 - a/3b)]$ where J_c is in A cm^{-2}, ΔM is magnetization hysteresis during increasing and decreasing field processes in emu cm^{-3}, and a, b ($a < b$) are cross-sectional sample dimensions (in cm) in the plain perpendicular to the applied field [30]. Magnetic field dependence of the critical current densities at 50 K and 77 K are shown in Fig. 3 for doping ratios of $x = 0.00$, 0.05, 0.10, 0.15, 0.20, 0.25 and 0.35. For all the doped-samples in Fig. 3(a) J_c at 50 K monotonically increases with increasing doping ratio up to $x = 0.25$ and decreases with increasing applied field between 0 and 0.5 T generally. At 50 K a shoulder-like feature also appears in each curve when $0.00 \leq x \leq 0.25$. This feature indicates field-induced pinning centers in Yb211-doped bulk Sm123 superconductor. As shown in Fig. 3, the maximum value of J_c at zero field decreases with further increasing of x for $x > 0.25$ implying that $x = 0.25$ is the optimum Yb211 doping ratio.

In Fig. 3(b) at 77 K, almost all the samples except for doping ratio $x = 0.35$ and 0.25 show a partial secondary peak effect at an external field between ~0.51 – 1.21 T whereas J_c with doping ratio $x = 0.35$ has dropped abruptly to zero at about 1.5 T. In addition, it

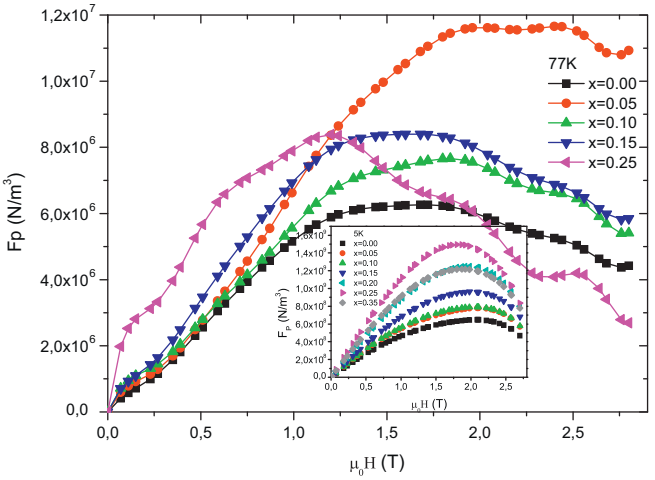

Fig. 4. Variation of volume pinning force F_p as a function of magnetic field of $(Sm123)_{1-x}(Yb211)_x$ sample for different Yb211 doping ratios at 77 K and 5 K (inset plot).

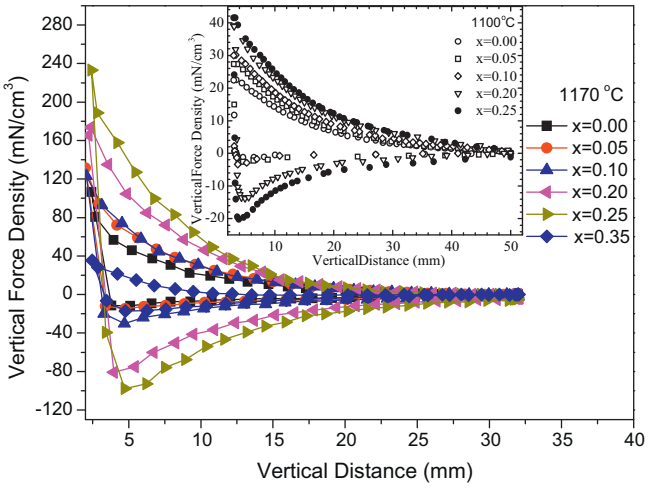

Fig. 5. The vertical levitation force density vs. vertical distance between the MPMG-processed $(Sm123)_{1-x}(Yb211)_x$ samples and the permanent magnet for reheat-temperatures at 1170 and 1100 °C (inset plot [29]).

is seen from Fig. 3 that for the doping ratio $x = 0.35$, J_c decreases continuously with increasing the magnetic field for both measurement temperatures at 50 and 77 K. At 77 K and for zero-field, the $(Sm123)_{1-x}(Yb211)_x$ sample with 0.25 doping ratio shows the best $J_c(0)$ value which is almost five times larger than that of the undoped one, whereas in the peak effect region the best J_c performance has the sample with Yb211 doping ratio of $x = 0.05$. This means that suitable amounts of Yb211 doping not only enhance J_c in the low field region but also in the high field region compared with undoped sample. This property of $(Sm123)_{1-x}(Yb211)_x$ samples make them attractive for applications under high magnetic field. In Fig. 3(b) for $x > 0.05$, the second peak moves to lower field with increasing of x doping ratio up to 0.20. For this case, it is suggested that the presence of the Yb123, (Sm,Yb)123 superconductors and Yb211 and $BaCuO_2$ non-superconducting phases in solid solution (as confirmed by SEM-EDX measurements) gives rise to compositional fluctuations. This leads to a spatial distribution of T_c in $(Sm123)_{1-x}(Yb211)_x$ superconductors, which provides the called δT_c pinning. It is known that this δT_c pinning is signaled by the second-peak effect in the $J_c(B)$ curves of superconductors [31]. For doping ratio $x > 0.05$ the increase of the non-superconducting phases amount in superconductor sample degrades the superconducting properties of the Sm123 matrix at 77 K and this leads to the reduction of δT_c pinning effects so that the value of J_c decreases in higher magnetic fields. In this study, the value of J_c at 77 K is lower than MPMG-processed Y123 with Ag addition and melt-textured (TSMG process) Sm123 with Sm242 addition, although the $J_c(0)$ value at 77 K of $(Sm123)_{1-x}(Yb211)_x$ sample for $x = 0.25$ is almost five times larger than that of the undoped sample. It can be thought that one of the reasons of the lower J_c in this sample are cracks in a/b-planes. It was reported that these cracks are formed because of mechanical stresses, which arise in the sample during its fabrication. Generally two main sources of stresses appearing during fabrication were suggested as the different thermal expansion coefficients of 123 and 211 phases (such as Sm123, Sm211 and Yb211) and the dependence of 123 phase lattice parameters on the oxygen stoichiometry [26,32]. It is well known that Ag particles significantly suppress cracking in superconductor sample because the addition of Ag improve the mechanical properties of 123/211 bulks [10,32]. It is suggested that other reasons of the lower J_c in $(Sm123)_{1-x}(Yb211)_x$ samples compared to melt-textured Sm123 with Sm242 [22] and nano-Sm211 (or nano-Nd422) additives [33] are the non-uniform distribution and large size of the Yb211 particles.

Fig. 4 shows the plot of the volume pinning force $F_p - B$ (in which $F_p = J_c \times B$ and $B = \mu_0 H$) curves at 77 K and 5 K (inset plot). It is seen from Fig. 4 the value of volume pinning force increase with increasing of doping ratio x at 5 K except for $x = 0.35$. The maximum volume pinning force at 5 K is $\sim 1.5 \times 10^9\ Nm^{-3}$ for $x = 0.25$ doping ratio which is approximately two times larger than undoped sample. F_p increases with increasing external magnetic field B in a low-field regime, after that F_p exhibits a maximum value in an intermediate field range and finally with further increasing field F_p decreases at 5 K. In addition, in this figure it is seen that, the peak position of the $F_{p\,max}$ is Yb211 doping ratio dependent since the peak position moves to lower field with increasing of x doping ratio. As in the case of J_c at 77 K in Fig. 3(b), the curves at 77 K in Fig. 4 show that the pinning force dependence on Yb211 doping ratio was not straightforward. In Fig. 4 it was observed that F_p increase generally with increasing doping ratio x compared with pure sample, except for the very strong increasing the doping ratio of $x = 0.05$ in the high field region. This implies that dominant pinning properties are different depending on the field quantity, measurement temperature and doping ratio. The non-superconducting phases such as Yb211 particles and crystal defects contribute to pinning in low field regions (δl pinning) with increasing Yb211 doping ratio. On the other hand the RE-rich low T_c clusters such as (Sm,Yb)123, the mixture of different RE211 clusters and nano-sized compositional fluctuation regions contribute to pinning (mentioned before as δT_c pinning) for optimum Yb211 doping ratio as $x = 0.05$ in high field region at 77 K. These regions were also known as field induced pinning centers and therefore enhance F_p and J_c in high magnetic field regions [25,28,34].

In this study in order to verify the pinning types [35] and obtain an insight into the origin of the pinning properties in the sample, an analysis up to 3 T was performed. Because of the improved superconductivity for Yb211 doped MPMG-processed Sm123 bulk, a detailed analysis (up to 6 T) will be carried out about the addition of the nano-scale Yb211, Sm211 and Ag phases into the TSMG-processed Sm123 single grains in the future.

Fig. 5 shows the vertical levitation force density (force per volume of HTS) as a function of vertical distance in ZFC state at $T = 77$ K for MPMG-processed $(Sm123)_{1-x}(Yb211)_x$ samples with different reheat-temperatures at 1170 and 1100 °C (inset plot [26]). Initially the samples are cooled with CH = 32 mm, then the vertical levitation force density vs. vertical distance is measured with a descending vertical traverse to 2 mm, followed by an ascending vertical traverse to 32 mm for samples with reheat-temperatures

at 1170 °C. As shown in Fig. 5, the vertical levitation force density increases as the PM moves toward the surface of the HTS and reaches the highest value for sample a reheat-temperature of 1170 °C and a Yb211 doping ratio $x = 0.25$. This value is approximately six times larger than that for a sample produced before at 1100 °C reheat-temperature [26]. In Fig. 5 the maximum vertical levitation force density increases with increasing of Yb211 doping level and reheat-temperature indicating enhanced pinning properties of the $(Sm123)_{1-x}(Yb211)_x$ sample for $x = 0.25$ at low magnetic fields. However, as confirmed from F_p curves, the best pinning properties at higher magnetic field than 1.2 T at 77 K were found for $(Sm123)_{1-x}(Yb211)_x$ samples with a doping ratio of $x = 0.05$.

4. Conclusion

The offset T_c, c-lattice parameter, $J_c(H)$, $F_p(H)$ curves, pinning mechanism and the vertical levitation force density properties of MPMG-processed $(Sm123)_{1-x}(Yb211)_x$ samples were investigated depending on Yb211 doping ratio. It was found that although the crystal structure of the samples kept their orthorhombic form, the value of c-lattice constant and T_c reduces with increasing x doping ratio. In $J_c(H)$ curves at 50 K a shoulder-like feature appears when $0.00 \leq x \leq 0.25$ reflecting the enhancement of J_c by Yb211 doping in the presence of magnetic field. At 77 K and low fields, $(Sm123)_{1-x}(Yb211)_x$ sample with 0.25 doping ratio shows the best $J_c(0)$ value which is almost five times larger than that of the undoped one. In contrast, in the peak effect region the best J_c performance has the sample with Yb211 doping ratio of $x = 0.05$. In addition, It was found that the vertical levitation force density increases as the PM moves toward the surface of the HTS and reaches the highest value for sample with reheat-temperature at 1170 °C and doping ratio for $x = 0.25$. This value is approximately six times larger than that obtained for sample reheated at 1100 °C reheat-temperature. By utilizing these properties of Yb211-doped Sm123 sample, various small and large-scale superconductor applications can be carried out by optimization the feature of compositional fluctuation regions, sample size and processing conditions of the Sm123 sample.

Acknowledgments

This work was supported by the Scientific and Technological Research Council of Turkey (TÜBITAK), with project No. 108T659 and partly the Scientific Research Project Fund of Karadeniz Technical University of Turkey, with project No. 2008.111.001.10.

References

[1] F.C. Moon, Superconducting Levitation, Wiley-VCH Verlag GmbH & Co. KGaA, Weinheim, 2004.
[2] J.R. Hull, Supercond. Sci. Technol. 13 (2000) R1–R15.
[3] Z. Wen, Y. Liu, W. Yang, M. Qiu, J. Phys. D: Appl. Phys. 40 (2007) 7281–7286.
[4] D. Dimos, P. Chaudhari, J. Mannhart, F.K. LeGoues, Phys. Rev. Lett. 61 (1988) 219–222.
[5] B. Martinez, X. Obradors, A. Gou, V. Gomis, S. Pinol, J. Fontcuberta, H. Van Tol, Phys. Rev. B 53 (1996) 2797–2810.
[6] S. Meslin, K. Iida, N.H. Babu, A.D. Cardwell, J.G. Noudem, Supercond. Sci. Technol. 19 (2006) 711–718.
[7] S. Jin, T.H. Tiefel, R.C. Sherwood, R.B. van Dover, M.E. Davis, G.W. Kammlott, R.A. Fastnacht, Phys. Rev. B 37 (1988) 7850–7853.
[8] M. Murakami, M. Morita, K. Doi, K. Miyamoto, Jpn. J. Appl. Phys. 28 (1989) 1189–1194.
[9] Y. Feng, A.K. Pradhan, Y. Zhao, Y. Wu, N. Koshizuka, L. Zhou, Physica C 357 (2001) 799–802.
[10] M. Murakami, T. Oyama, H. Fujimoto, S. Gotoh, K. Yamaguchi, Y. Shiohara, N. Koshizuoka, S. Tanaka, IEEE Trans. Magnet. 27 (1991) 1479–1486.
[11] S. Gruss, G. Fuchs, G. Krabbes, P. Verges, G. Stöver, K.H. Müller, J. Fink, L. Schultz, Appl. Phys. Lett. 79 (2001) 3131–3133.
[12] D.A. Cardwell, Mater. Sci. Eng. B 53 (1998) 1–10.
[13] A. Devi, V. Bai, P.V. Patanjall, R. Pinto, N. Kumar, S.K. Malik, Supercond. Sci. Technol. 13 (2000) 935–939.
[14] Ş. Çelik, K. Öztürk, E. Yanmaz, J. Alloys Compd. 456 (2008) 1–5.
[15] Y. Xu, M. Izumi, K. Tsuzuki, Y. Zhang, C. Xu, M. Murakami, N. Sakai, I. Hirabayashi, Supercond. Sci. Technol. 22 (2009), 095009 (6pp).
[16] K. Öztürk, Ş. Çelik, U. Çevik, E. Yanmaz, J. Alloys Compd. 456 (2008) 34–39.
[17] N.H. Babu, K. Iida, D.A. Cardwell, Supercond. Sci. Technol. 20 (2007) S141–S146.
[18] C. Xu, A. Hu, N. Sakai, M. Izumi, I. Hirabayashi, Supercond. Sci. Technol. 18 (2005) 1082–1088.
[19] I.G. Chen, F.C. Chang, M.K. Wu, Supercond. Sci. Technol. 15 (2002) 717–721.
[20] M. Muralidhar, N. Sakai, N. Chikumoto, M. Jirsa, T. Machi, M. Nishiyama, Y. Wu, M. Murakami, Phys. Rev. Lett. 89 (2002), 237001 (4pp).
[21] F. Giovannelli, J. Noudem, D. Brouri, D. Bourgault, I. Monot-Laffez, Supercond. Sci. Technol. 18 (2005) S149–S152.
[22] L. Sun, W. Li, S. Liu, T. Mertelj, X. Yao, Supercond. Sci. Technol. 22 (2009), 125008 (6pp).
[23] J.L. MacManus-Driscoll, J.A.G. Nelstrop, A. Berenov, X. Qi, Physica C 384 (2003) 507–513.
[24] Y. Li, G.K. Perkins, A.D. Caplin, G.H. Cao, Q.Z. Ma, L. Wei, Z.X. Zhao, Physica C 341 (2000) 2037–2038.
[25] S.Y. Chen, I.G. Chen, M.K. Wu, Supercond. Sci. Technol. 18 (2005) 916–920.
[26] K. Ozturk, S. Celik, A. Cansiz, Phys. Status Solidi A 206 (2009) 2569–2575.
[27] S. Çelik, K. Ozturk, Phys. Status Solidi A 206 (2009) 724–730.
[28] M. Murakami, N. Sakai, T. Higuchi, S.I. Yoo, Supercond. Sci. Technol. 9 (1996) 1015–1032.
[29] R. Kita, K. Yokoyama, Physica C 392 (2003) 488–492.
[30] E.M. Gyorgy, R.B. van Dover, K.A. Jackson, L.F. Schneemeyer, J.V. Waszczak, Appl. Phys. Lett. 55 (1989) 283–285.
[31] H. Zhang, Y. Liu, H.L. Li, J.F. Qu, X.G. Li, Y. Feng, Supercond. Sci. Technol. 18 (2005) 1317–1322.
[32] P. Diko, Supercond. Sci. Technol. 17 (2004) R45–R58.
[33] P.C. Hsieh, S.Y. Chen, I.G. Chen, M.K. Wu, Supercond. Sci. Technol. 18 (2005) S111–S118.
[34] S.Y. Chen, A. Gloter, C. Colliex, I.G. Chen, M.K. Wu, IEEE Trans. Appl. Supercond. 17 (2007) 2957–2960.
[35] T. Goto, K. Inagaki, K. Watanabe, Physica C 330 (2000) 51–57.